JOURNAL OF MATERIALS SCIENCE 32 (1997) 2181–2189

Preparation and phase transformations of melt-spun Al–Ge–Si brazing foils

TH. SCHUBERT, W. LÖSER, A. TERESIAK, N. MATTERN, H.-D. BAUER
Institut für Festkörper- und Werkstofforschung Dresden, Postfach 270016 D-01171 Dresden, Germany

A series of Al–Ge–Si alloys was melt spun into ribbons of about 40 μm thickness. The alloy compositions were selected so as to be suitable as filler metals with brazing temperatures $< 500\,^{\circ}C$. In the as-quenched state the foils were relatively brittle due to the occurrence of metastable phases. After appropriate annealing treatments between 300–400 °C the metastable phases were transformed into a fine-grained microstructure of β-Ge(Si) particles within the α-Al matrix. This led to considerably improved mechanical properties, which are manifested in decreased microhardness levels near 100 $HV_{0.02}$ and bend radii < 1 mm. The transformation process of foils on annealing was investigated by differential scanning calorimetry, transmission electron microscopy and X-ray diffraction methods. The intensity of X-ray reflections of the metastable and equilibrium phases as well as the lattice parameters of α-Al and β-Ge(Si) were evaluated as functions of the annealing temperature. Differences in the transformation behaviour of binary Al–Ge and ternary Al–Ge–Si alloys, in particular, the decreased transformation temperature for the decay of metastable phases in ternary alloys, were revealed.

1. Introduction

The production of brazing and soldering foils by melt spinning is an example of the successful application of rapid solidification technology [1–3]. The main advantages of melt spun brazing foils are (I) preparation of ductile amorphous or microcrystalline foils of otherwise brittle alloy compositions, (II) their superior homogeneity and fine-grained microstructure and (III) the absence of any organic binder in the filler materials [1]. Notwithstanding the wide variety of melt-spun brazing foils produced there are still demands for new filler metal compositions for special purposes. The interest in Al–Ge–Si alloys arises from the current use of AlSi12 eutectic alloys in two fields of application: (I) brazing of Al alloys [1, 2, 4, 5], and (II) applications in high-power semiconducting devices (brazing of silicon wafers to molybdenum) [6, 7]. The application of Al–Ge–Si ternary alloys instead of AlSi12 filler metals allows the development of lower melting brazing foils, since the Al–Ge–Si alloy system is characterized by a single monovariant eutectic valley running down from the AlSi12.7 binary eutectic at $T_E = 577\,^{\circ}C$ to the AlGe53 binary eutectic at $T_E = 424\,^{\circ}C$ [8]. Al–Ge–Si based filler metals of appropriate compositions with melting temperatures below 500 °C will permit lower processing temperatures during brazing. This will reduce mismatch stresses in semiconducting device assemblies [6, 7] and, alternatively, the degradation of microstructure and mechanical properties in the joining of high-performance Al alloys for aerospace applications.

The preparation of ductile Al–Ge–Si foils by rapid solidification methods is hampered by the formation of brittle metastable phases, which have been extensively investigated in the binary Al–Ge system [9–14]. In a previous paper a processing route for ductile Al–Ge soldering foils for electronic applications was described which combined melt spinning with an appropriate annealing of as-cast ribbons [15].

The present investigation is devoted to establishing methods for the preparation of ductile low melting Al–Ge–Si brazing foils. The phase content of as-quenched Al–Ge–Si foils prepared by melt spinning is revealed by transmission electron microscopy (TEM) and X-ray investigations and compared with that of binary Al–Ge alloys. The phase transformation behaviour on isochronal annealing is studied by X-ray methods and related to the change in mechanical properties of the foils.

2. Experimental procedure

Master alloys AlGe45, AlGe45Si2 and AlGe45Si4 (in wt %) were prepared from aluminium of 99.999% purity and germanium and silicon of semiconductor purity in an induction furnace and cast into rods. Ingots of 30 g were cast into thin ribbons of about 40 μm thickness and 10 mm width on an experimental melt spinning facility with a copper wheel 200 mm in diameter.

In order to characterize the mechanical behaviour of the ribbons, microhardness measurements and

0022–2461

bending tests were performed on selected samples. The melting behaviour of the alloys was studied by differential scanning calorimetry (DSC) scans with a heating rate of $10\,K\,min^{-1}$ utilizing the Perkin-Elmer DSC7 calorimeter. Accompanying investigations of the microstructure of the as-quenched ribbons were performed by analytical transmission electron microscopy. Therefore, the ribbon material was thinned up to electron transparency by Ar-ion bombardment of 3–5 keV with 5–7° incidence angle by means of the ion-etching device Gatan 691 PIPS. Care had to be taken for a sufficient thermal contact between the sample and holder, in order to exclude undesired phase transformations during the thinning process. Using the Philips CM 20-FEG microscope at a beam voltage of 200 kV conventional micrographs and diffraction diagrams have been produced, the latter from regions of diameters <100 nm. For the study of the element distribution spectra and mappings are made by means of an energy dispersive X-ray spectrometer (EDX) Tracor Voyager IIa with a HPGe detector.

Thermal reactions caused by transformations of possible metastable phases were revealed on heating of samples in the as-quenched state. Specimens of approximately 50 mg were analysed in a Netzsch (model DSC 404) differential scanning calorimeter using a heating rate of $20\,K\,min^{-1}$. The thermal analyses were performed in conjunction with X-ray diffraction to permit the identification of corresponding phases at different stages of the transformation process. The diffraction patterns of the samples were recorded by means of a Stoe diffractometer with Co-K_α radiation and a primary Ge-monochromator. In addition, diffraction patterns recorded by a Philips PW 1050 diffractometer were used to determine lattice parameters of the Al and Ge phases and to study the decomposition of the supersaturated matrix in the rapidly solidified ribbons as a function of temperature.

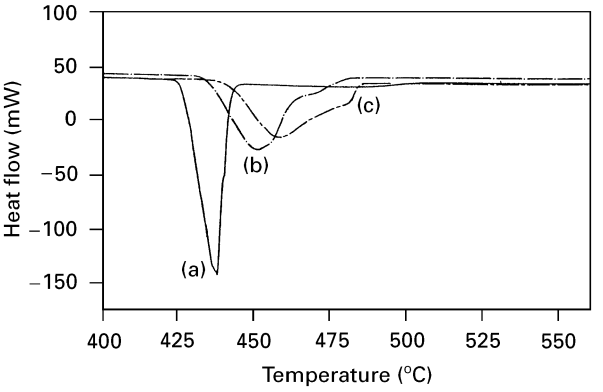

Figure 1 DSC scans with heating rates of $10\,K\,min^{-1}$ demonstrating the melting behaviour of the (a) AlGe45, (b) AlGe45Si2 and (c) AlGe45Si4 alloys.

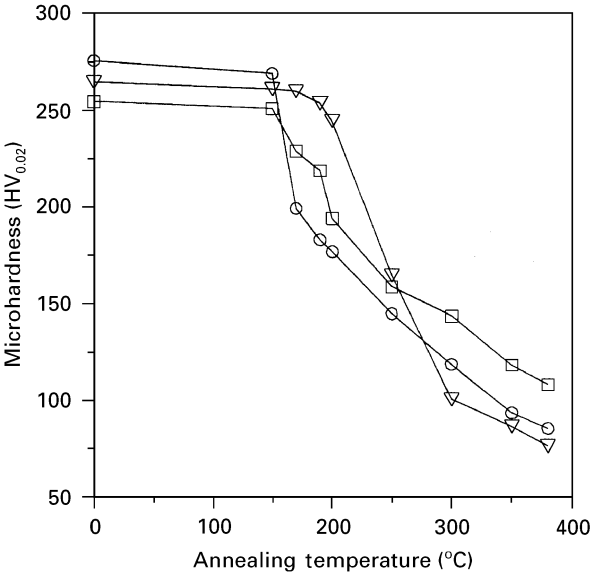

Figure 2 Microhardness results $HV_{0,02}$ of (▽) AlGe45, (○) AlGe45Si2 and (□) AlGe45Si4 alloy ribbons in the as-quenched state and after 1.8 ks isothermal annealing as a function of annealing temperature.

3. Results

3.1. DSC and microhardness measurements

The three alloy compositions chosen represent a section through the ternary eutectic trough slightly below the binary eutectic composition AlGe53 [8]. The DSC scans characterizing the melting behaviour of all three alloys are displayed in Fig. 1. The onset temperature of 425 °C of the AlGe45 alloy, which is very near the reported melting temperature of the binary Al–Ge eutectic, is shifted to slightly higher temperatures of 433 °C (AlGe45Si2) and 437 °C (AlGe45Si4), respectively, for ternary alloys. Increasing silicon contents cause a change of the melting interval of the alloys, and the end-points of the melting process are shifted from 501 °C (AlGe45) to 496 °C (AlGe45Si2) and 557 °C (AlGe45Si4). Since brazing can commonly be performed in the two-phase range of the filler metals (melt + primary solid phase) the alloys should be suitable for brazing temperatures below 500 °C or even 450 °C (AlGe45) [15].

The as-cast ribbons of all three alloy compositions are extremly brittle (a microhardness of about 270 $HV_{0.02}$) in agreement with earlier results [15]. However, by subsequent annealing the ductility of the as-quenched ribbons can be substantially improved. As demonstrated in Fig. 2 for isothermal annealing of 1.8 ks at different temperatures ranging between 150–380 °C the microhardness changes from its initial value near 270 $HV_{0.02}$ by annealing and attains ultimate values of about 78 $HV_{0.02}$ (AlGe45), 85 $HV_{0.02}$ (AlGe45Si2) and 110 $HV_{0.02}$ (AlGe45Si4) at 380 °C. As is shown in Fig. 2 the slope of the microhardness occurs at lower annealing temperatures for ternary alloys but the ultimate hardness levels are enhanced by alloying with silicon. In the final state, after annealing for 1.8 ks at 380 °C, 40 μm thick ribbons of the binary AlGe45 alloy can be bent 180° with a bend radius $r = 0$ without fracture, whereas the ternary alloys exhibit finite bend radii of $r \approx 0.5$ mm (AlGe45Si2) and $r \approx 0.7$ mm (AlGe45Si4), respectively, as is shown in Fig. 3. In all cases the annealed ribbons can be cut and punched.

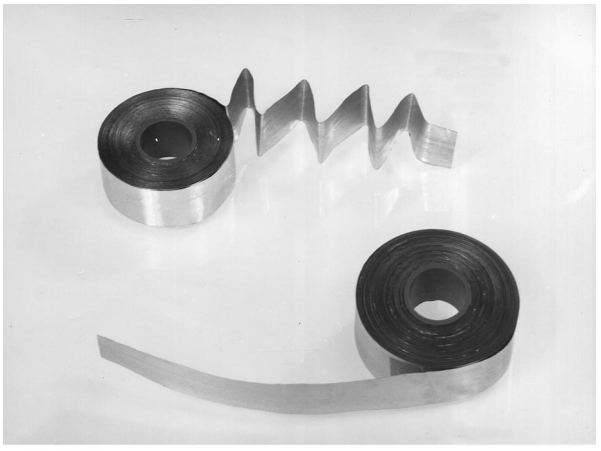

Figure 3 Viewgraph of a coil of ductile AlGe45Si2 ribbon annealed 1.8 ks at 380 °C wound on a core of 10 mm diameter displaying several bends without fractures.

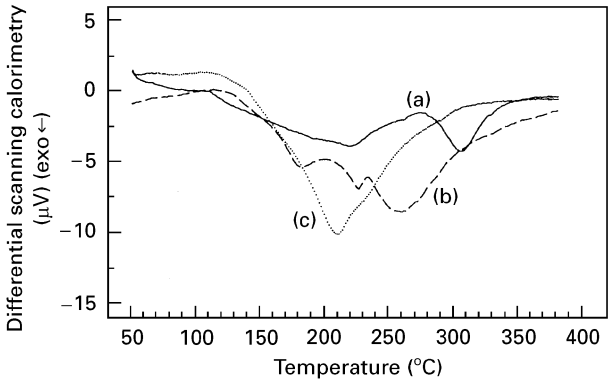

Figure 4 DSC characteristics of the solid state transformation behaviour of as-quenched (a) AlGe45, (b) AlGe45Si2 and (c) AlGe45Si4 alloy ribbons on isochronal annealing with heating rates of 20 K min^{-1} showing exothermal peaks typically for the decay of metastable phases.

From the isochronal DSC scans shown in Fig. 4 one can clearly distinguish some differences between the solid state transformations for the binary alloy AlGe45 and for the ternary alloys AlGe45Si2 and AlGe45Si4. In binary Al–Ge alloys the transformation process consists of two steps with distinct exothermal peak temperatures near 220 °C and 305 °C in accordance with Laridjani *et al.* [13] who ascribed them to the decomposition of the metastable γ_1 and γ_2 intermetallic phases. The increasing silicon content accelerates this transformation process and reduces the transformation temperatures. Therefore only a fused single peak near 210 °C was revealed in the DSC plot of the ternary AlGe45Si4 alloy. In both binary and ternary alloys there is a wide temperature interval of 200 K for completion of the transformation process if heating rates of 20 K min^{-1} are applied.

3.2. TEM investigations

TEM analysis was performed to obtain information on the influence of Si on the microstructure of as-quenched specimens. Fig. 5 displays the type of micro-

Figure 5 Bright field electron micrograph of a typical region in the AlGe45 as-quenched ribbon.

structure which was most frequently observed in the thin foils made from the binary AlGe45 alloy ribbons. Evidently, there exists a dendritic structure surrounded by a primary cellular phase.

In addition, EDX-microanalyses (Fig. 6(a and b)) show, that the maximum Al-content in the brighter regions is accompanied by a depletion of Ge, whereas the dark-looking parts of the eutectic mixture are enriched with Ge and depleted in Al. Selected area diffraction (SAD) patterns obtained from these different phases could be indexed as α-Al in the case of the brighter Al-rich regions (Fig. 7a) and as the metastable phases γ_1 and γ_2 in the case of the darker Ge-rich regions (Fig. 7b). These results are in good agreement with previous structural investigations reported by Köster [11, 16] and Kaufman and Fraser [14].

When the AlGe45Si2 alloy ribbons were examined the observed microstructure was more refined but of similar appearance to that of the AlGe45 alloy (Fig. 8). In contrast to the binary alloy ribbons the electron diffraction patterns provide evidence for the formation of some β-Ge particles in addition to α-Al and the metastable γ_1 and γ_2 phases in the as-quenched state (Fig. 9(a and b)). Again, EDX analysis was used to reveal the spatial distribution of Si shown in Fig. 10(a–c). It is evident, that Si is predominantly found at the regions which are enriched with Ge. Therefore, this result implies a co-segregation of Ge and Si atoms in both the metastable phases and the fine-dispersed β-Ge particles.

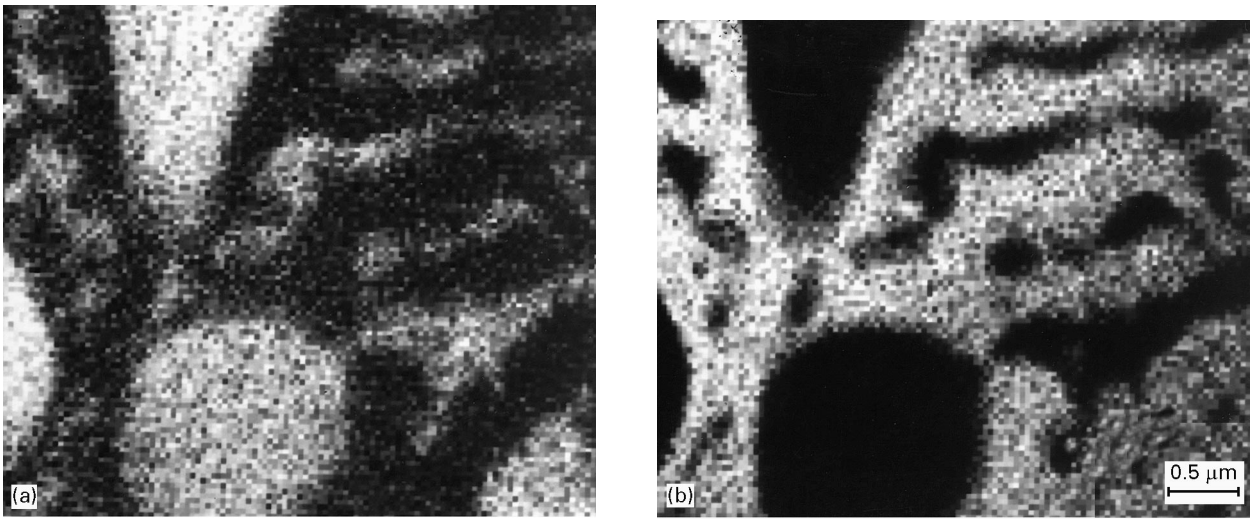

Figure 6 Element distribution mappings of (a) aluminium and (b) germanium in AlGe45 as-quenched ribbons.

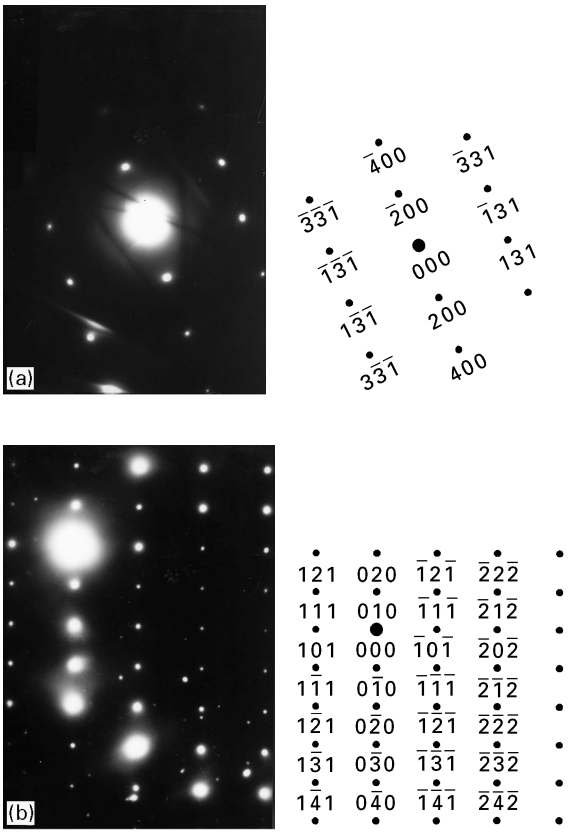

Figure 7 SAD patterns from (a) the α-Al phase (in [013] zone axis orientation) and (b) the monoclinic γ_2-phase as an example of the metastable phases (in [101] zone axis orientation).

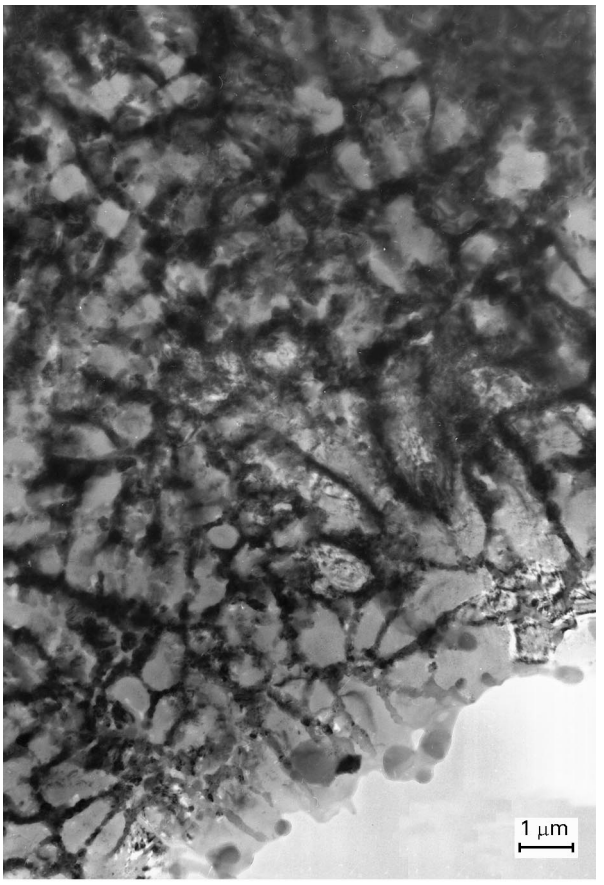

Figure 8 Bright field electron micrograph of a typical region in the AlGe45Si2 as-quenched ribbon.

3.3. X-ray investigations

The X-ray diffraction patterns of as-quenched and annealed samples were evaluated to obtain structural information regarding the observed phase transformations. The annealing process was performed by a stepwise temperature increase from room temperature in 25 K intervals with a rate of 20 K per min up to 400 °C. At any temperature level after a dwelltime of 2 min the samples were exposed to X-rays for 5 min in order to derive the diffraction patterns. In Fig. 11a reflections of the metastable γ_1 and γ_2 phases in addition to those of the supersaturated α-Al phase are shown to occur in the as-quenched state and for annealing temperatures $T_a \leqslant 275$ °C. The crystal structure of rapidly quenched Al–Ge alloys has been investigated by numerous authors and interpreted by deriving structural models [9–14]. In our work, the metastable rhombohedral structured γ_1 phase and the monoclinic structured γ_2 phase were clearly identified in the as-quenched state in the binary Al–Ge as well as

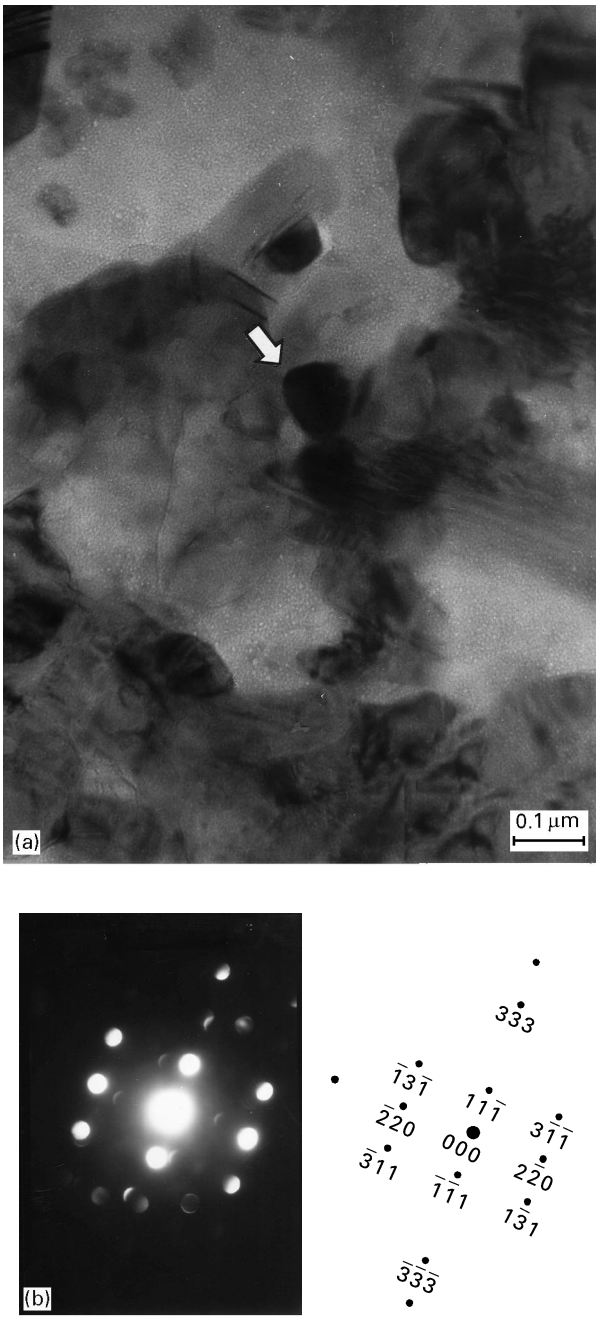

Figure 9 β-Ge(Si) particle in the AlGe45Si2 as-quenched ribbon: (a) bright field electron micrograph and (b) SAD pattern (in [112] zone axis orientation).

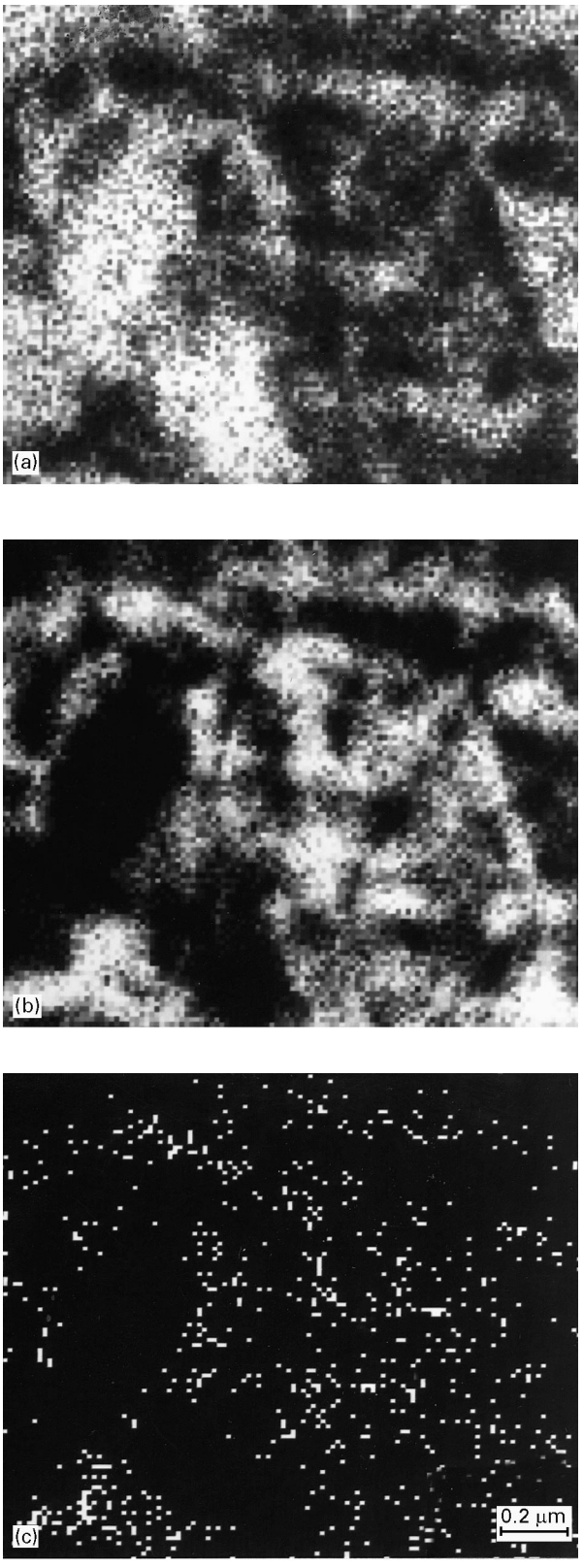

Figure 10 Element distribution mappings of (a) aluminium, (b) germanium and (c) silicon in AlGe45Si2 as-quenched ribbons.

in the ternary Al–Ge–Si alloys, Fig. 11b. Annealing of the specimens leads to a gradual decay of the metastable phases indicated by the disappearance of the corresponding reflections. Obviously, the transformation of the metastable phases is connected with a simultaneous intensity gain of the α-Al and β-Ge(Si) reflections.

A more conclusive representation of the dependence of the transformation behaviour on annealing temperature is presented in Figs 12–14 that show the X-ray intensities of the constituent phases of the three different alloys (derived from the strongest reflection of each phase). The binary AlGe45 alloy, Fig. 12, exhibits three phases in the as-quenched state: α-Al solid solution, the rhombohedral (γ_1) and the monoclinic (γ_2) phases. The decay of the metastable phases proceeds between 240–300 °C with no distinct difference between the transformation temperatures of the γ_1 and γ_2 phases. The reflections of both metastable phases were always found to be simultaneously reduced in contradiction to the finding of Laridjani *et al.* [13]. The intensity of the α-Al increased in this range of temperature, but the most striking feature is the sudden appearance of a significant intensity for β-Ge at

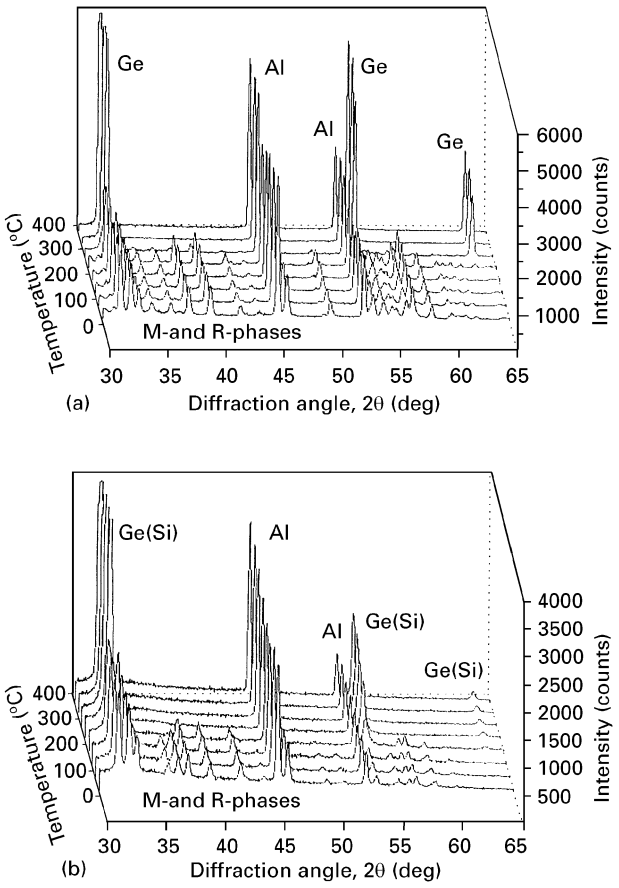

Figure 11 X-ray powder diffraction intensities as a function of diffraction angle for (a) AlGe45 and (b) AlGe45Si2 as-quenched alloys showing the decay of the metastable γ_1-(R) and γ_2-(M) phases with increasing annealing temperatures from 50–400 °C.

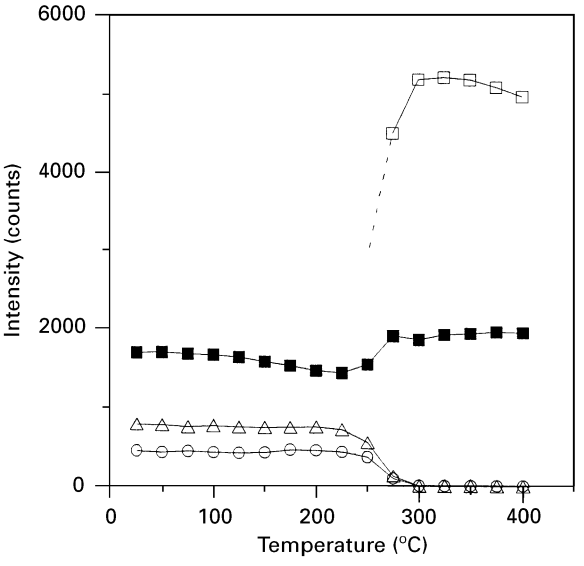

Figure 12 X-ray intensities of the constituent phases of binary AlGe45 foils as function of the annealing temperature. Key: (□) Ge, (■) Al, (△) R phase and (○) M phase.

temperatures near 280 °C. Quantitative phase analysis shows that after cooling to room temperature the specimens consist of 53.5 ± 2.0 wt % α-Al and 46.5 ± 2.0 wt % β-Ge.

Alloying with 2 wt % Si lowers the transformation temperatures of the γ_1 and γ_2 phases by more than

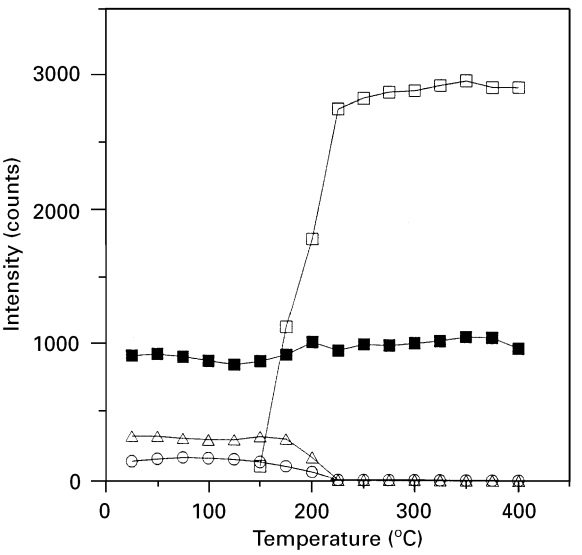

Figure 13 X-ray intensities of the constituent phases of ternary AlGe45Si2 foils as function of the annealing temperature. Key: (□) Ge, (■) Al, (△) R phase and (○) M phase.

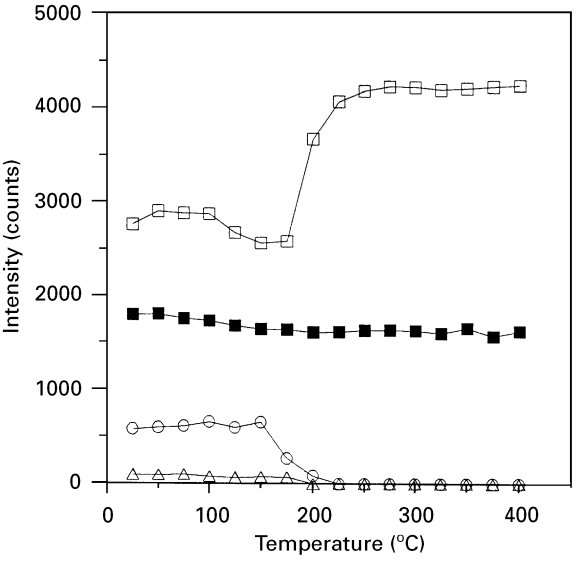

Figure 14 X-ray intensities of the constituent phases of ternary AlGe45Si4 foils as function of the annealing temperature. Key: (□) Ge, (■) Al, (△) R phase and (○) M phase.

50 K. As is shown in Fig. 13 the decomposition of the metastable phases in the AlGe45Si2 alloy near 180 °C is accompanied by a small increase of the α-Al intensity and a vast increase in the β-Ge intensity. A further increase in silicon content leads to the occurrence of the β-Ge phase in the as-quenched state as demonstrated for the AlGe45Si4 alloy in Fig. 14. The fraction of the rhombohedral γ_1-phase is reduced to a marginal quantity and transformation temperatures are shifted to values near 160 °C.

Evaluation of the lattice parameters of the α-Al and β-Ge phases provides further insight into the structural transformation of the alloys with different compositions. The lattice constant characteristics as a function of annealing temperature for the α-Al(Ge) phase, presented in Fig. 15, reflect both thermal

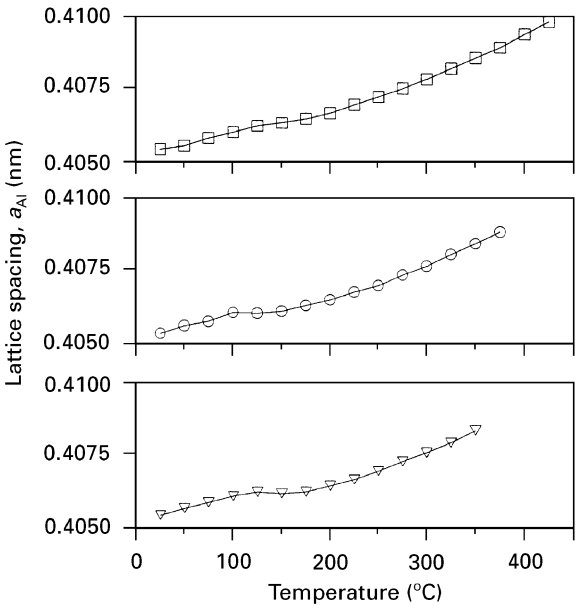

Figure 15 Lattice parameter of the α-Al phase as a function of temperature for the three different alloy compositions (▽) AlGe45, (○) AlGe45Si2 and (□) AlGe45Si4.

expansion as well as supersaturated solute solution effects inherent to rapid solidification methods.

An average thermal expansion coefficient of $da/dT = 26 \times 10^{-6}\,K^{-1}$ can be estimated from the slopes of the experimental curves in Fig. 15, which is in reasonable agreement with the published values for α-Al [17].

The presence of Ge in solid solution will increase the α-Al lattice constant whereas Si will reduce it. The solute content of germanium and silicon in α-Al(Ge) was estimated using an X-ray diffraction technique with an internal silicon standard. Utilizing the known lattice spacing for pure aluminium ($a_{Al} = 0.40496$ nm) [18] and the lattice parameters determined for the α-Al(Ge) solid solution (0.40554 ± 0.00008) nm in as-quenched AlGe45 specimens a supersaturation of 3.5 at % Ge was estimated by extrapolating the Axon- and Hume-Ruthery line [19]. This value agrees with the result reported by Laridjani [20]. Generally, the α-Al lattice parameter is smaller for ternary Al–Ge–Si alloys compared with the binary Al–Ge alloys. The corresponding lattice parameters (0.40530 ± 0.00008) nm and (0.40527 ± 0.00008) nm in AlGe45Si2 and AlGe45Si4, respectively, are lowered by 0.00024 and 0.00027 nm in comparison to that of the binary alloy. This effect can be due to both a smaller amount of Ge dissolved or additional Si solute in ternary AlGeSi alloys. These effects cannot be separated by the X-ray investigations. The TEM results presented imply, that in the case of AlGe45Si2 this effect can be explained by assuming a reduced solid solubility of Ge in α-Al(Ge), because (I) the element distribution mappings show predominantly a combination of Ge with Si atoms in the metastable phases and (II) isolated Ge particles were found in the as-quenched state. On this basis a smaller metastable germanium solid solubility of 2 at % Ge can be estimated for α-Al(Ge) of the ternary alloy. Due to their small volume fraction the β-Ge precipitates formed could not be detected by X-ray methods in the as-quenched AlGe45Si2 ribbons. In AlGe45Si4 ribbons it can be assumed that the decrease of a_{Al} is also caused by a smaller Ge-content in solid solution, because about 25 wt % of precipitated β-Ge is already observed in the as-quenched state.

As demonstrated in Fig. 15, there is one striking change in slope in the lattice parameter versus temperature characteristic of the binary AlGe45 alloy in the temperature range of 130–180 °C which may be attributed to the Ge solute dilution in the supersaturated α-Al(Ge) matrix. For AlGe45Si2 alloys the corresponding change in slope is shifted to lower temperatures between 100–150 °C. The thermal expansion effect of the α-Al lattice constant in AlGe45Si4 is slightly retarded in the temperature range of 120–180 °C, but this effect is not so apparent as for the other alloys. This fact closely corresponds to the lower supersaturation due to the precipitated β-Ge in the as-quenched state as shown in Fig. 14. The room temperature α-Al lattice constant is reduced to an identical value of (0.40520 ± 0.00002) nm for all three alloys due to the loss of solute, but it is slightly enhanced compared to that of pure Al. The α-Al lattice constant is possibly influenced by internal stresses due to the different thermal expansions of Al and Ge [21].

The lattice constant versus annealing temperature characteristics of the β-Ge(Si) phase, presented in Fig. 16, manifest considerable differences between the binary Al–Ge and ternary Al–Ge–Si alloy ribbons. For binary AlGe45 the lattice spacing of β-Ge smoothly increases with temperature after the appearance of the first Ge-reflections at 280 °C. This behaviour indicates the thermal expansion of β-Ge with $da/dT = 6 \times 10^{-6}\,K^{-1}$ in good agreement with the results of Pearson [17]. After cooling to room temperature the value of elemental Ge $a_{Ge} = (0.56565 \pm 0.00002)$ nm is found. The characteristics of the ternary Al–Ge–Si alloys display a more intricate behaviour. The lattice constant of the β-Ge(Si) phase

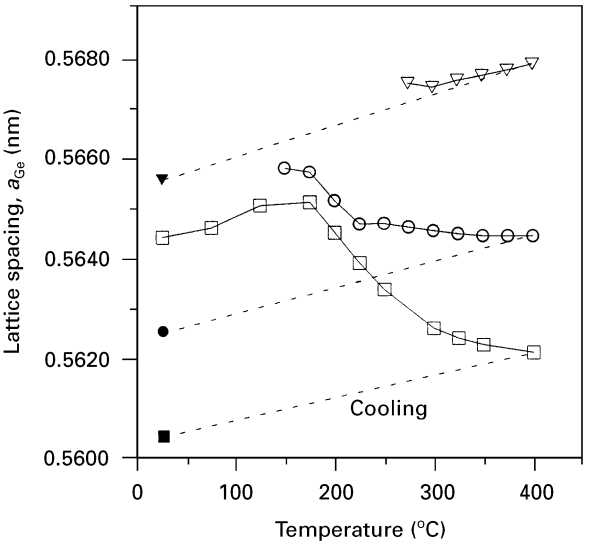

Figure 16 Lattice parameter of the β-Ge phase as a function of temperature for the three different alloy compositions (▽) AlGe45, (○) AlGe45Si2 and (□) AlGe45Si4. The filled symbols indicate the lattice parameters after recovery to room-temperature.

in AlGe45Si2 alloys decreases with rising temperature from a maximum value just after detection of the β-Ge(Si) phase near 150 °C. In AlGe45Si4 alloys the β-Ge(Si) lattice parameter first increases with temperature and then drops after the peak value near 150 °C is approached. After recovery to room temperature the β-Ge(Si) lattice parameter is shown to decrease in the sequence of increasing silicon content reflecting the expected behaviour from the equilibrium phase diagram, which predicts a complete solid solubility of Si in β-Ge. The remaining silicon is dissolved in the β-Ge(Si) phase causing a reduction of the corresponding lattice parameter from $a_{Ge} = (0.56565 \pm 0.00002)$ nm in AlGe45 to $a_{Ge} = (0.56278 \pm 0.00002)$ nm and $a_{Ge} = (0.56062 \pm 0.00002)$ nm determined in the melt-spun ternary alloys AlGe45Si2 and AlGe45Si4, respectively. A considerable time is required to approach phase equilibrium on the annealing of Al–Ge–Si foils at elevated temperatures. The observed temperature characteristics of the β-Ge(Si) lattice parameter indicate a simultaneous precipitation of Ge and Si, which has previously been described for conventional solidification as the coring effect [8]. The homogeneous β-Ge(Si) phase is then formed by interdiffusion at elevated temperature.

4. Discussion

The determination of the microhardness and bending radii along with the phase transformation behaviour on annealing lead to the conclusion that the embrittlement of the as-quenched Al–Ge–Si ribbons can be attributed to the occurrence of metastable intermetallic phases resembling those formed in rapidly solidified binary Al–Ge alloys [9–15]. It was shown that the detrimental effect produced by these metastable phases on the mechanical behaviour can be overcome by appropriate annealing beyond the composition-dependent decomposition temperature of the metastable phases. The microstructure of ductile ribbons after the decay of metastable phases into the equilibrium phases upon annealing displays fine disperse β-Ge(Si) particles embedded in the ductile α-Al matrix (Fig. 17). This two-phase morphology is the key to the improved mechanical behaviour and contrasts with the coarse branched network of the brittle β-Ge(Si)-phase obtained after conventional solidification [8, 22].

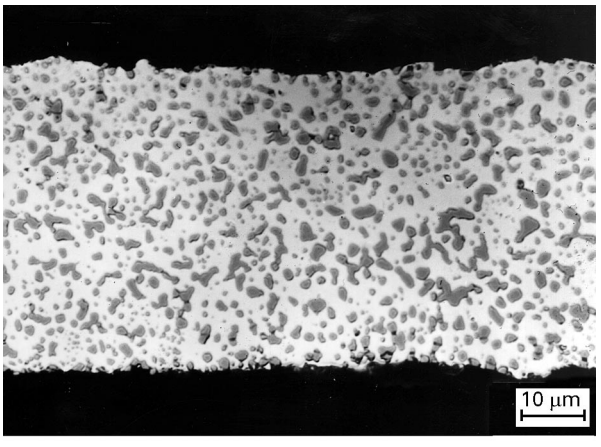

Figure 17 Typical micrograph of a AlGe45Si2 ribbon, annealed for 1.8 ks at 400 °C: aluminium – bright, germanium – dark.

All the investigated alloys exhibit a transformation $\gamma_1; \gamma_2 \rightarrow$ α-Al + β-Ge(Si) upon annealing. In addition, there is no clear distinction between the transformation temperatures of the metastable γ_1 and γ_2 phases as claimed in a previous paper on the basis of DSC measurements in binary Al–Ge alloys [12, 13]. *In-situ* investigations of the isochronal transformation behaviour at 20 K min^{-1} with synchrotron radiation confirmed our conclusion concerning the transformation temperatures of the metastable phases [23]. According to our X-ray results the low temperature DSC peak, which is rather significant in binary Al–Ge alloys, can be ascribed to the decay of the supersaturated α-Al(Ge) solid solution prior to the decomposition of the metastable phases. The corresponding transition temperature near 150 °C derived from lattice parameter determination of α-Al(Ge) closely agrees with the results of Köster [16] for precipitation in solid state quenched Al–Ge alloys.

The main effects of silicon on the Al–Ge–Si foils are the reduction of the metastable phase fraction and the depression of the transformation temperature for the decomposition of the metastable phases. It is well known, that unlike Al–Ge alloys, Al–Si alloys have not been reported to form metastable intermetallic compounds [24–26]. Therefore, our results imply, that the small Si-contents reduce the driving forces for the formation of these nonequilibrium structures in rapidly quenched ternary Al–Ge–Si alloys compared with binary Al–Ge alloys.

In addition, the solid state transformation kinetics may itself be influenced by the presence of a ternary element. Köster [11, 16] observed, that the decomposition process of the metastable phases in binary Al–Ge ribbons starts with the precipitation of β-Ge and proceeds by the diffusion of Ge from the metastable phases to these β-Ge precipitates. Accordingly, for the ternary Al–Ge–Si alloys investigated here we expect that the transformation process in the as-quenched ribbons upon annealing is accompanied by the precipitation of β-Ge(Si) particles in contrast to pure β-Ge in the binary alloy AlGe45. Our X-ray studies provide some evidence for the existence of such β-Ge(Si) precipitates. But, it was shown, that the precipitation behaviour in Al–Ge–Si alloys is different from binary Al–Ge alloys. Hornbogen [27] found a higher density of nuclei in water-quenched and aged low-alloyed Al–Ge–Si alloys. This effect was explained by pair formation of Ge and Si atoms and nucleation of covalently bonded (Ge, Si) particles from clusters in the metallic Al-matrix. The coprecipitation of larger Ge atoms with smaller Si atoms should reduce the strain energy in the fcc Al-matrix resulting in the higher density of nuclei. Therefore the decomposition kinetics of the metastable phases in ternary Al–Ge–Si alloy ribbons will be promoted by the presence of Si. In addition, the microhardness determinations in Fig. 1 let us conclude, that there is no kinetic advantage for the transformation of the ternary alloys for higher annealing temperatures, i.e., in the advanced stages of transformation.

The precipitation behaviour will be investigated in more detail by electron microscopic investigations, that will be reported in a future publication.

5. Conclusion

Notwithstanding the differences in the transformation kinetics it was shown that ductile foils of both binary Al–Ge and ternary Al–Ge–Si alloys can be prepared by melt spinning and subsequent annealing. After the decay of the metastable phases the foils display a fine-grained microstructure of β-Ge(Si) particles in the α-Al matrix, and improved mechanical properties. The foils, which are suitable as filler metals for temperatures as low as 500 °C, can be further improved with respect to their brazing behaviour by additional alloying components.

Acknowledgements

The authors are indebted to Mrs S. Schinnerling, Mrs U. Kühn, Mrs B. Arnold, Mrs D. Bieberstein and Mr W. Gude for technical assistance, and Professor H. Warlimont for valuable discussions. Thanks also have to be given to GATAN Inc., München, for the temporary loan of a PIPS-machine.

References

1. N. J. DeCRISTOFARO and A. DATTA, in "Rapidly quenched metals", edited by S. Steeb and H. Warlimont (Elsevier, Amsterdam, 1985) p. 1715.
2. N. J. DeCRISTOFARO and D. BOSE, in Proceedings of the ASM Int. Conf. on Rapidly Solidified Materials, San Diego (CA) 3–5 Feb 1986, edited by P. W. Lee and R. S. Carbonara (ASM, Metals Park, OH, 1986) p. 415.
3. A. RABINKIN and H. H. LIEBERMANN, in "Rapidly solidified alloys – processes, structures, properties, applications", edited by H. H. Liebermann (Marcel Dekker, New York, 1993) p. 691.
4. J. W. WERNER, US Patent 3 697 259 (1972).
5. W. TILLMANN and E. LUGSCHEIDER, *Schweißen und Schneiden* **46** (1994) 543.
6. D. M. JACOBSON and G. HUMPSTON, *Met. Mater.* **7** (1991) 733.
7. F. H. HAYES, R. D. LONGBOTTOM, E. AHMAD and G. CHEN, *J. Phase Equilibria* **14** (1993) 425.
8. H. SONG and A. HELLAWELL, *Metall. Trans. A* **21A** (1990) 733.
9. C. SURYANARAYANA and T. R. ANANTHARAMAN, *J. Mater. Sci.* **5** (1970) 992.
10. *Idem*, *Metallography* **4** (1971) 79.
11. U. KÖSTER, *Z. Metallkde.* **63** (1972) 472.
12. P. RAMACHANDRARAO, M. G. SCOTT and G. A. CHADWICK, *Phil. Mag.* **25** (1972) 961.
13. M. LARIDJANI, K. D. KRISHNANAND and R. W. CAHN, *J. Mater. Sci.* **11** (1976) 1643.
14. M. J. KAUFMAN and H. L. FRASER, *Acta Metall.* **33** (1985) 191.
15. L. ILLGEN, H. MÜHLBACH, W. LÖSER, H. G. LINDENKREUZ, E. ALIUS, D. RÜLICKE and M. MÜLLER, *Mater. Sci. Engng.* **A133** (1991) 738.
16. U. KÖSTER, Ph.D. thesis, Göttingen (1971).
17. W. B. PEARSON, "A handbook of lattice spacings and structures of metals and alloys" (Pergamon, London, 1967).
18. Powder Diffraction Standard Data Base PDF-2, International Centre of Diffraction Data, Swarthmore, PA.
19. H. J. AXON and W. HUME-ROTHERY, *Proc. Roy. Soc.* **A193** (1948) 1.
20. M. LARIDJANI, *Mater. Sci. Engng.* **23** (1976) 125.
21. E. J. MITTEMEIJER, P. VAN MOURIK, TH. H. DE KEIJSER, *Phil. Mag. A* **43** (1981) 1157.
22. A. HELLAWELL, *Trans. Metall. Soc. of AIME* **239** (1967) 1049.
23. N. MATTERN, A. TERESIAK, T. SCHUBERT, W. LÖSER and S. DOYLE, *Powder Diffraction* (submitted).
24. A. BENDIJK, R. DELHEZ, L. KATGERMAN, TH. H. KEIJSER, E. J. MITTEMEIJER and N. M. VAN DER PERS, *J. Mater. Sci.* **15** (1980) 2803.
25. A.-M. PAPON and S. PAIDASSI, in Proceedings of the ASM Int. Conf. on Rapidly Solidified Materials, San Diego (CA) 3–5 Feb 1986, edited by P. W. Lee and R. S. Carbonara (ASM, Metals Park, OH, 1986) p. 317.
26. S. DAS, A. H. YEGNESWARAN and P. K. ROHATGI, *J. Mater. Sci.* **22** (1987) 3173.
27. E. HORNBOGEN, A. K. MUKHOPADHYAY and E. A. STARKE Jr., *Z. Metallkde* **83** (1992) 577.

Received 10 April 1995
and accepted 21 October 1996